

A Comparison for Patch-level Classification of Deep Learning Methods on Transparent Environmental Microorganism Images: from Convolutional Neural Networks to Visual Transformers

Hechen Yang^a, Chen Li^{a,*}, Jinghua Zhang^a, Peng Zhao^a, Ao Chen^a, Xin Zhao^b, Tao Jiang^c and Marcin Grzegorzek^d

^aMicroscopic Image and Medical Image Analysis Group, MBIE College, Northeastern University, 110169, Shenyang, PR China

^bEnvironmental Engineering Department, Northeastern University, Shenyang 110169, China

^cSchool of Control Engineering, Chengdu University of Information Technology, Chengdu 610225, China

^dInstitute of Medical Informatics, University of Luebeck, Luebeck, Germany

ARTICLE INFO

Keywords:

Patch Level
Image Classification
Transparent Images
Deep Learning
Convolutional Neural Network
Visual Transformer
Environmental Microorganism

ABSTRACT

Nowadays, analysis of *Transparent Environmental Microorganism Images* (T-EM images) in the field of computer vision has gradually become a new and interesting spot. This paper compares different deep learning classification performance for the problem that T-EM images are challenging to analyze. We crop the T-EM images into 8×8 and 224×224 pixel patches in the same proportion and then divide the two different pixel patches into foreground and background according to ground truth. We also use four convolutional neural networks and a novel ViT network model to compare the foreground and background classification experiments. We conclude that ViT performs the worst in classifying 8×8 pixel patches, but it outperforms most convolutional neural networks in classifying 224×224 pixel patches.

1. Introduction

Nowadays in industrialized countries, environmental pollution is an essential problem, and microorganisms are closely related to environmental protection and sustainable development. *Environmental Microorganisms* (EMs) are tiny living beings in natural or artificial environments, which are invisible to the naked eye (their size usually varies between 0.1 and 100 μm) and they can only be observed under microscopes. EMs are natural decomposers and indicators and they can solve environmental pollution without any secondary pollution. For example, *Actinophrys* can digest organic waste in sludge and improve the quality of fresh water. Therefore, EMs plays an important role in solving the problem of environmental pollution.


There are four traditional methods for EM identification. The first one is physical method. This method has high accuracy in identifying EMs but requires expensive equipment. The second is chemical method, which has a high accuracy rate but often prone to cause secondary pollution. The third method is molecular biology recognizes EMs through the sequence of genes. However, it requires professional researchers and expensive equipment. The fourth method is morphological observation, which requires experienced operators to observe the EMs under a microscope and it requires a lot of manpower and energy. Therefore, these four methods have their shortcomings in actual operation. Therefore, we consider that the excellent performance of deep learning in the field of image processing can be used to make up for the shortcomings of traditional methods.

In EMs, there are many categories that are transparent and colorless, resulting a lot of difficulties in the EM image

analysis process. Nowadays, the application of *Transparent Environmental Microorganism Images* (T-EM images) has become more and more widely used in various fields around humans. Such as, identifying the number of EMs in the environment to judge the degree of environmental pollution [1]. In recent years, the detection of transparent objects in images is also a hot spot in vision research. It is not an easy task to detect whether there are transparent objects or translucent objects in images [2]. Because the transparent target area to be observed is generally very small or very thin, the colors and contrast of foreground and background are similar, and only the residual edge part leads to the low resolution of foreground or background, which largely depends on its background and lighting conditions. Therefore, there is an urgent need for some effective methods to identify transparent or translucent EM images.

In recent years, computer vision has good performance in computer vision acquisition [3], contour tracking [4], edge detection [5], face recognition [6], fingerprint recognition [7], automatic driving [8], and medical image analysis [9]. We considering the excellent performance of computer vision in image analysis, such as high speed, high accuracy, low consumption, high degree of quantification, strong objectivity [10], therefore computer vision can make up the shortcomings of traditional morphological methods. It brings new opportunities to EM images analysis. Especially when an image is transparent and short of visual information, we usually need to crop it into patches to discover more visual details to recover the lost information. Hence, research work on patch-level is significant for transparent image analysis, such as patch-level image segmentation and classification tasks.

In recent years, deep learning is the most efficient method in the field of machine vision, such as the popular *Convolutional*

 lichen201096@hotmail.com (C. Li)

tional Neural Network (CNN) Xception [11], VGG-16 [12], Resnet50 [13], Inception-V3 [14], MobileNet [15], NasNet [16], and novel *Visual Transformers* (VTs) [17]. CNNs slowly expand the receptive field until it covers the whole image by accumulating convolution layers, so CNNs complete the extraction of graphics from local to global information. In contrast, transformers can obtain global information from the beginning, so they are more difficult to learn, but their ability to learn long-term dependence is stronger [17]. Hence, CNNs and Transformers have advantages and disadvantages in dealing with visual information. Therefore, this paper compares the patch-level classification performance of transparent images with different CNN and VT methods, where it aims to discover the adaptability of different deep learning models in this research domain.

This paper uses EMDS-5 as an example of T-EM images. First, the transparent images are divided into training, validation, and test sets according to a ratio of 2:2:4. The workflow of patch-level image classification is shown in Fig. 1, where (a) is the training set, including original images and ground truth (GT) images with multi-scale settings. (b) is the training process of deep learning models where several typical deep learning methods are selected and trained. (c) is the test set. (d) is the patch-level classification prediction result.

The structure of this paper is as follows: In Section 2, related work about deep learning in the classification of T-EM images is introduced. In Section 3, comparative experiments about T-EM image classification on multi-scale patches with deep learning methods are carried out. In Section 4, the conclusion and future work about T-EM images are summarized in the patch-level classification of deep learning methods results and the future development of deep learning methods for analyzing T-EM images.

2. Related Work

First, this section introduces the application scenarios of EM. Next, we introduce some common analysis methods, application scenarios, and research purposes of transparent object images. Finally, the advantages and disadvantages of some popular deep learning methods are also discussed.

2.1. Introduction to Environment Microorganism

The study of EM is essential in the progress of human society and the development of civilization. EM are involved in most areas of humans. In the industrial field, the treatment of industrial wastewater is an important issue to protect the environment. Due to the presence of carbohydrates, fats, proteins and other organic matter in wastewater, which are food for EM. EMs can convert organic matter into less complex compounds and neutralize toxic substances[18]. Therefore, EMs effectively degrading harmful substances in industrial wastewater. In the medical field, some EMs with pathogens can bring diseases to humans and cause death. However, people also use these microorganisms to create many seedlings to prevent these diseases, so that the human body has resistance to certain diseases, which has played a

key role in the development of medicine[19]. In the agricultural field, the metabolites of some EMs can be used as natural biological pesticides. People use its characteristics to produce agricultural products including pesticides, herbicides, fertilizers and so on. In addition, the *Paramecium* in the rice fields can purify sewage to improve the survival rate of crops and increase production[20]. In the ecological field, *rotifers* can decompose the garbage in the water and reduce the degree of eutrophication, thereby improving the quality of water. Moreover, *rotifers* are good biological food for fry growth, which play an important role in balancing the aquatic ecosystem[21]. In the food field, the *yeast* can be used to make puffed food, edible vinegar, and wine making[22].

2.2. Introduction to Transparent Object Image Analysis

Object analysis is one of the essential branches in robot vision, especially the analysis of transparent images of objects (transparent object images) is challenging [23]. In traditional machine analysis methods, the flexibility of transparent object image features obtained by integrating multi-class algorithms is poor, and performance is difficult to improve. For example, home robots can not see things at all when they are detecting some transparent glassware. The ClearGrasp machine learning algorithm performs well in analyzing transparent objects [24]. It can estimate high-precision data of transparent objects from RGB-D transparent images, thereby improving the accuracy of transparent object detection.

As a necessary technical means for analyzing objects, photoelectric sensors are widely used in industrial automation, mechanization, and intelligence. It uses the properties of light to detect the position and change of the object, but when detecting transparent color objects, the light beam of the traditional diffuse reflection photoelectric sensor penetrates the transparent material, causing the sensor to fail. Diffuse reflection photoelectric sensor adopts a phase-locked loop narrowband filter frequency selection technology, which improves the sensitivity to self-returning light and stability of detecting transparent objects [25].

There are many transparent objects in the industrial field, such as transparent plastics, transparent colloids, and liquid drops. These transparent objects bring much uncertainty to products. If factories want to have high-quality products, sometimes it is essential to analyze these transparent objects and control the shapes of the transparent objects. However, it is a difficult problem to segmentation the shape of transparent objects through morphological methods. For instance, Hata et al. used a genetic algorithm to segmentation the transparent paste drop shape in the industry and obtained good performance [26].

The segmentation of transparent objects is very useful in computer vision applications. However, the foreground of a transparent image is usually similar to its background environment, which leads to the general image segmentation methods in dealing with transparent images in general.

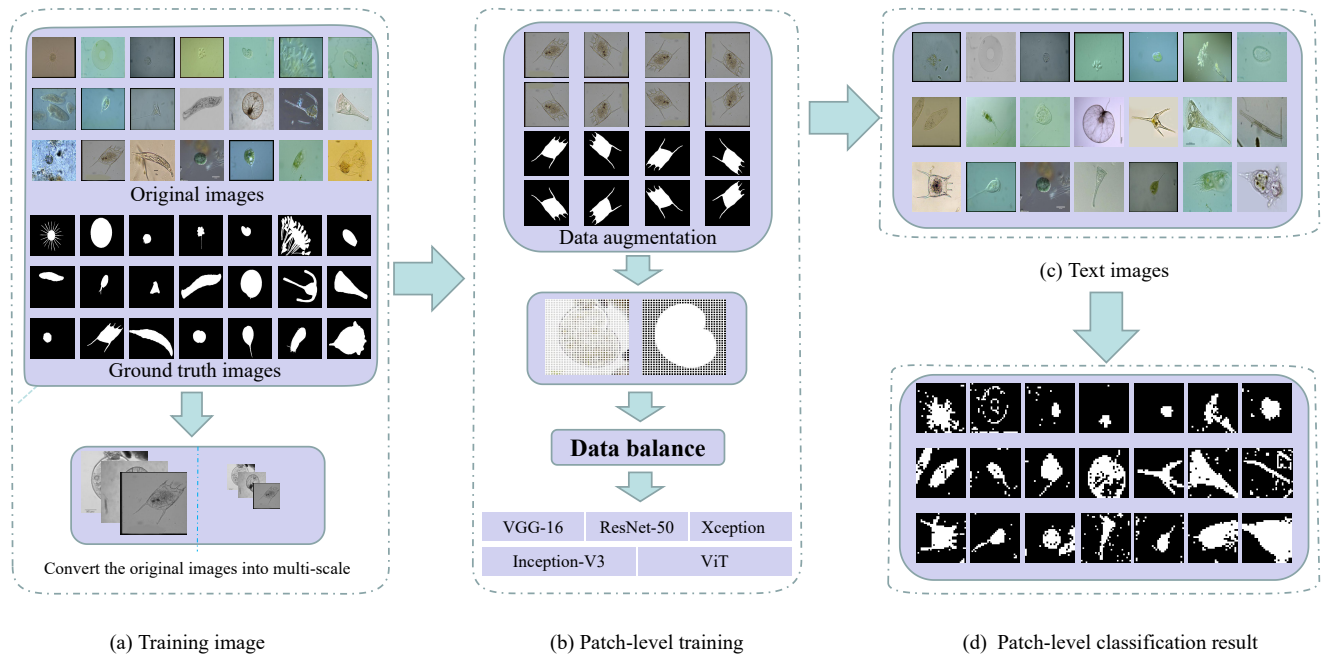


Figure 1: Workflow of patch-level classification in T-EM images (using environmental microorganism EMDS-5 images as examples).

The light field image segmentation method can accurately and automatically segment transparent object images with a small depth of field difference and improve the accuracy of the segmentation, and it has a small amount of calculation [27]. Hence, it is widely used in the segmentation of transparent object images.

The correct segmentation of zebrafish in biology has extensively promoted the development of life sciences. However, the zebrafish's transparency makes the edges blurred in the segmentation. The mean shift algorithm can enhance the color representation in the image and improve the discrimination of the specimen against the background [28]. This method improves the efficiency and accuracy of zebrafish specimen segmentation.

Visual object classification is vital for robotics and computer vision applications. Commonly used statistical classification methods such as bag-of-features [29] are often applied to image classification. The principle is to extract local features of the image for classification. However, these methods cannot be applied to the classification of transparent images because transparent object images largely depend on the background. Foreground transparent objects do not have their complete characteristics, and it is not easy to classify them accurately. The more popular method is the light field distortion feature [30], which can describe transparent objects without knowing the texture of the scene, thus improving the accuracy of classifying transparent object images.

2.3. Deep Learning

Simonyan et al. propose the VGG series of deep learning network models (VGG-Net), of which VGG-16 is the most representative [31]. VGG-Net can imitate a larger receptive field by using multiple 3×3 filters, enhancing nonlinear mapping, reducing parameters, and improving the network to be more judgmental. Meanwhile, VGG-16 continues to deepen the previous VGG-Net, with 13 convolutional layers and three fully connected layers. With the continuous increase of convolution kernel and convolution layer, the nonlinear ability of the model is stronger. VGG-16 can better learn the features in images and achieve good performance in analyzing image classification, segmentation, and detection. Simonyan proves that as the depth of the network increases, it promotes the accuracy of image analysis [31]. Nevertheless, this increase in depth is not without a limit. Excessively increasing the depth of the network will lead to network degradation problems. Therefore, the optimal network depth of VGG-Net is set to 16-19 layers. Moreover, VGG-16 has three fully connected layers, which causes more memory to be occupied, too long training time, and difficulty in tuning parameters.

He et al. propose the ResNet series of networks and add a residual structure in networks to solve the problem of network degradation [32]. The ResNet model introduces a jumpy connection method "shortcut connection". This connection method allows the residual structure to skip some levels that not be fully trained in the feature extraction process and increases the model's utilization of feature information during the training process. As the most classical

model in the ResNet series, ResNet50 has a 50-layer network structure. This model adopts the highway network structure, which makes the network have strong expression capabilities and the ability to acquire more advanced features. Therefore, it is widely used in the field of image analysis. However, the network model is too deep and complicated, so how to judge which layers in the deep network not be fully trained and then optimize the network is a complex problem.

Szegedy et al. propose the GoogLeNet network model, which has the advantage of reducing the complexity of the network based on ResNet. They first proposed Inception-v1, whose network is 22 layers deep and consists of multiple Inception structures cascade as basic modules. Each Inception module consists of a 1×1 , 3×3 , 5×5 convolution kernel and a 3×3 maximum pooling, which is similar to the idea of multi-scale and increases the adaptability of the network to different scales [33]. With the continuous improvement of the inception module, the inception-v2 network uses two 3×3 convolutions instead of 5×5 convolutions and increases the BN method, which reduces the amount of calculation and speeds up the training time [34]. The Inception-v3 network introduces the idea of decomposing convolution, splitting a larger two-dimensional convolution into two smaller one-dimensional convolutions, further reducing the amount of calculation [35]. At the same time, Inception-v3 optimizes the Inception module, embeds the branch in the branch and improves the model’s accuracy.

Xception is another improvement after Inception-v3 [36]. It mainly uses depthwise separable convolution to replace the convolution operation in Inception-v3. The Xception model uses deep separable convolution to increase the width of the network, which not only improves the accuracy of classification but also improves the ability to learn subtle features. Meanwhile, Xception adds a residual mechanism similar to ResNet to significantly improve the speed of convergence during training and the model’s accuracy. However, Xception is relatively fragmented in the calculation process, which results in a slower iteration speed during training.

Transformer is a deep neural network based on the self-attention mechanism, which enables the model to be trained in parallel and obtain the training data’s global information. Due to its computational efficiency and scalability, it is widely used in Natural Language Processing. Recently, Dosovitskiy et al. proposed the Vision Transformer (ViT) model and found that it performs very well on image classification tasks [37]. In the first step of training, the ViT model divides pictures into fixed-size image patches and uses its linear sequence as the input of the transformer model. In the second step, position embeddings are added to the embeddings patches to retain the position information, and then the image features are extracted through the multi-head attention mechanism. Finally, the classification model is trained. ViT breaks through the limitation that RNN model cannot be calculated in parallel, and self-attention can produce a more interpretable model. ViT is suitable for solving image processing tasks, but experiments have proved that large data samples are needed to improve the training effect.

Table 1
EMDS-5 Experimental data.

| | Training Set | Validation Set | Test Set |
|--------------------|--------------|----------------|----------|
| <i>Actinophrys</i> | 5 | 5 | 10 |
| <i>Arcella</i> | 5 | 5 | 10 |
| <i>Aspidisca</i> | 5 | 5 | 10 |
| <i>Codosiga</i> | 5 | 5 | 10 |
| <i>Colpoda</i> | 5 | 5 | 10 |
| <i>Epistylis</i> | 5 | 5 | 10 |
| <i>Euglypha</i> | 5 | 5 | 10 |
| <i>Paramecium</i> | 5 | 5 | 10 |
| <i>Rotifera</i> | 5 | 5 | 10 |
| <i>Vorticella</i> | 5 | 5 | 10 |
| <i>Noctiluca</i> | 5 | 5 | 10 |
| <i>Ceratium</i> | 5 | 5 | 10 |
| <i>Stentor</i> | 5 | 5 | 10 |
| <i>Siprostomum</i> | 5 | 5 | 10 |
| <i>K.Quadrata</i> | 5 | 5 | 10 |
| <i>Euglena</i> | 5 | 5 | 10 |
| <i>Gymnodinium</i> | 5 | 5 | 10 |
| <i>Gonyaulax</i> | 5 | 5 | 10 |
| <i>Phacus</i> | 5 | 5 | 10 |
| <i>Stylonychia</i> | 5 | 5 | 10 |
| <i>Synchaeta</i> | 5 | 5 | 10 |
| total | 105 | 105 | 210 |

2.4. Summary

T-EM image analysis is used in various fields, but the foreground and background of EM transparent images are too similar to make analysis difficult. Compared with deep learning methods, the general traditional analysis methods are time-consuming, labor-intensive, and costly. So this paper compares the performance of several classical deep learning networks for T-EM image analysis.

3. Comparative Experiment

This section introduces the patch-level classification experiment and classification results of T-EM images under several deep learning networks.

3.1. Experiment Setting

3.1.1. Data Settings

In our work, we use EM Data Set Fifth Version (EMDS-5) as T-EM images for analysis [1]. It is a newly released version of the EMDS series, which contains 21 types of EM, each of which contains 20 original microscopic images and their corresponding ground truth (GT) images (examples are shown in Fig.2 and Fig. 3). We randomly divide each category of EMDS-5 into training, validation, and test data sets at a ratio of 1:1:2. Therefore, as shown in Tab.1, we have 105 original images and their corresponding GT images for training and validation, respectively, and 210 original images for testing.

3.1.2. Data Preprocessing

In the first step, we uniformly convert all images sizes to 224×224 pixels and 7168×7168 pixels to keep that each im-

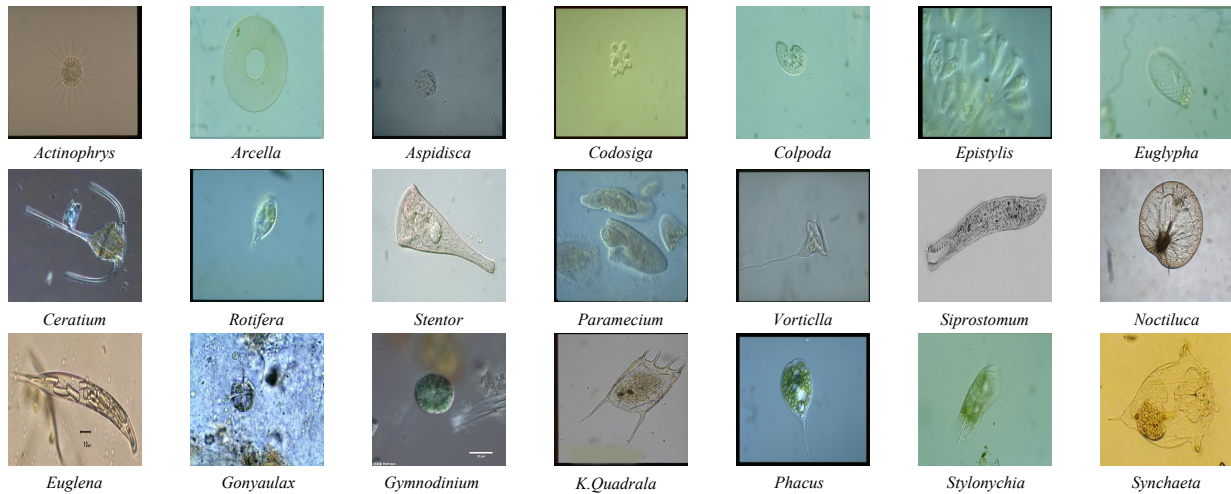


Figure 2: Examples of the environmental microorganism image in EMDS-5.

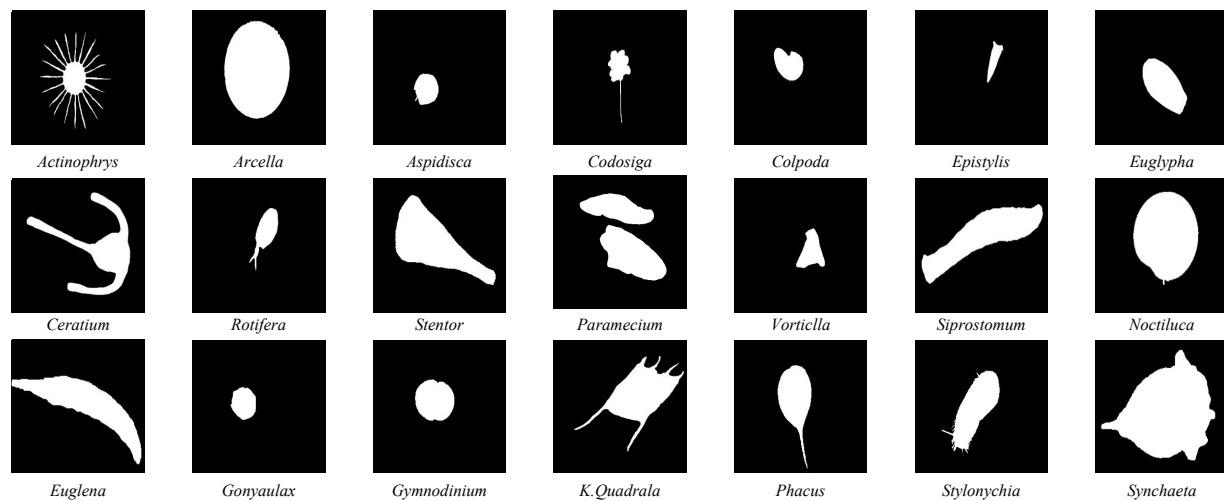


Figure 3: Environmental microorganism EMDS-5 ground truth images.

age is cropped into the same number of multi-scale patches. In the second step, we gray-scale EMDS-5 images to facilitate the calculation of gradients and feature extraction during training. In the third step, the training and validation images, and their corresponding GT images are cropped into patches (8×8 pixels and 224×224 pixels), where $105 \times 1024 = 107520$ patches are obtained. We divide these small patches into two categories according to the corresponding GT image small patches: foreground and background. The partition criterion is whether the target area in the patch takes up half of the whole patch. If it is, we will assign foreground as the label of this patch; otherwise, it will be background. In the fourth step, we find that the 224×224 pixel patches with foreground and background are 16630 and 90890, respectively. In order to avoid data imbalance during training, we rotate the training set image small patches by 0, 90, 180, 270 degrees and mirror them for data augmentation. Then we further obtain $16630 \times 8 = 133040$ patches, from which 90890 patches are

randomly selected as the finally used patches in the training set. We expand the data of the 8×8 pixel patches according to the same process. The details of the augmented data are provided in Tab. 2.

3.1.3. Experimental Environment

Our classification comparison experiment is conducted on a local computer with Win10 Professional operating system, and the computer has 16 GB RAM i7-10700 CPU and 8 GB NVIDIA Quadro RTX 4000 GPU. The CNN models we use in this paper are based on the Keras 2.3.1 framework using Tensorflow 2.0.0 as the backend; in the ViT model, we use the Pytorch 1.7.1 and Torchvision 8.0.2 operating environment.

3.1.4. Hyper Parameters

This experiment uses the Adam optimizer with a 0.0002 learning rate and sets the batch size to 32 in our training pro-

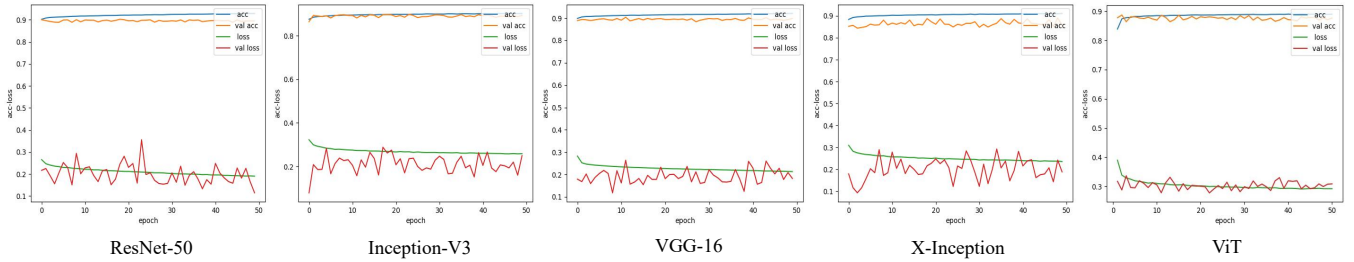


Figure 4: Compare the results of the loss and accuracy curves of deep learning on the 8×8 pixels training and the validation sets.

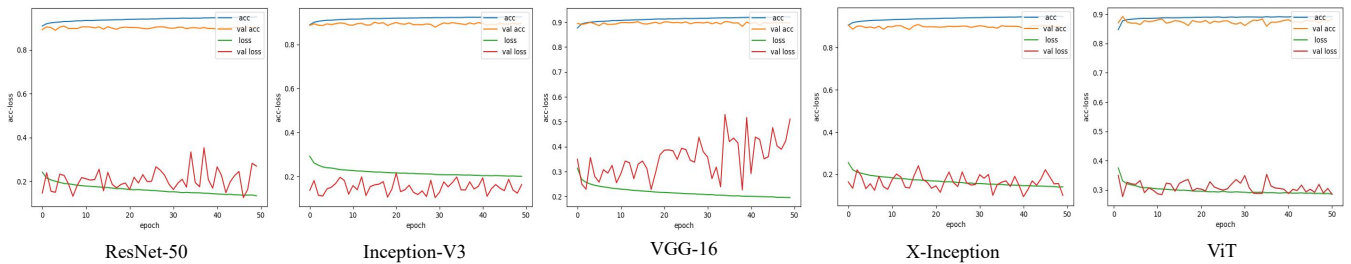


Figure 5: Compare the results of the loss and accuracy curves of deep learning on the 224×224 pixels training and the validation sets.

Table 2
Data augmentation. FG (foreground) and BG (background)

| Data Set | Training Set | Validation Set |
|---------------------------|--------------|----------------|
| 8×8 pixel FG | 16554 | 17356 |
| 8×8 pixel BG | 90966 | 90164 |
| Augmentation With FG | 90966 | \ |
| 8×8 Total | 181932 | 107520 |
| 224×224 pixel FG | 16630 | 17459 |
| 224×224 pixel BG | 90890 | 90061 |
| Augmentation With FG | 90890 | \ |
| 224×224 Total | 181780 | 107520 |

cess. In Fig. 4 and Fig. 5 show the accuracy and loss curves of different deep learning models in this experiment. We find that the loss and accuracy curves of the training set are converging after training for 40 layers. Therefore, considering the computational performance of the workstation, we finally set 50 epochs for training.

3.2. Evaluation Metrics

To compare the classification performance of different methods, we used the commonly used deep learning classification indexes Accuracy (Acc), Precision (Pre), Recall (Rec), Specificity (Spe), and F1-Score (F1) to evaluate the classification results. Acc reflects the ratio of correct classification samples to total samples. Pre reflects the proportion of correctly predict positive samples in the positive samples of model classification. Rec reflects the correct proportion of model classification in total positive samples. Spe reflects the proportion of the model correctly classifying the negative samples in the total negative samples. F1 is a calculation result that comprehensively considers the Pre and Rec of the model. These evaluation indexes are defined in Tab. 3. TP (True Positive), FN (False Negative), FP (False Positive), and TN (True Negative) are concepts in the confusion matrix.

3.3. Comparative Experiment

3.3.1. Comparative Experiment of 8×8 Pixel Patches Comparison on Training and Validation Sets: In order to compare the classification performance of CNNs and ViT models, we calculate Pre, Rec, Spe, F1, Acc, Max Acc. In Tab. 4, we summarize the results of 8×8 pixel patches on the validation set for each model. Overall, the Pre of the deep learning network in classifying the T-EM image backgrounds is higher than the foreground. Besides, the Pre of the five models to classify T-EM image backgrounds is almost 97%, the highest is the VGG-16 value of 97.6%, and

Table 3
Evaluation metrics for images classification.

| Assessments | Formula |
|-------------|-----------------------------------|
| Acc | $\frac{TP+TN}{TP+TN+FP+FN}$ |
| Pre | $\frac{TP}{TP+FP}$ |
| Rec | $\frac{TP}{TP+FN}$ |
| Spe | $\frac{TN}{TN+FP}$ |
| F1 | $2 \times \frac{P \times R}{P+R}$ |

Table 4
A comparison of the classification results on validation set of 8×8 pixel patches. MAcc (Max Acc), FG (foreground) and BG (background) (In [%]).

| Model | Class | Pre | Rec | Spe | F1 | MAcc |
|--------------|-------|------|------|------|------|-------|
| ResNet50 | FG | 62.3 | 88.2 | 89.7 | 73.0 | 92.87 |
| | BG | 97.5 | 89.7 | 88.2 | 93.4 | |
| Inception-V3 | FG | 61.8 | 88.6 | 89.5 | 72.8 | 90.24 |
| | BG | 97.6 | 89.5 | 88.6 | 93.4 | |
| VGG-16 | FG | 63.1 | 88.6 | 90.0 | 73.7 | 92.09 |
| | BG | 97.6 | 90.0 | 88.6 | 93.6 | |
| X-Inception | FG | 53.3 | 89.2 | 85.0 | 66.7 | 91.10 |
| | BG | 96.7 | 85.0 | 89.2 | 90.9 | |
| ViT | FG | 62.4 | 84.1 | 90.3 | 71.6 | 89.26 |
| | BG | 96.7 | 90.3 | 84.1 | 93.4 | |

the lowest is the X-Inception and the ViT value of 96.7%. Meanwhile, the Pre rate of classification foreground VGG-16 is the best and the Pre rate is 63.1%. The Inception-V3 obtains the lowest 53.3%. For T-EM image foregrounds classification, the highest Rec rate is obtained with X-Inception, which is 89.2%, and the lowest one is ViT, which is 84.1%. For T-EM image backgrounds classification, the highest Rec rate is the ViT value of 90.3% and the lowest is the X-Inception value of 85.0%. The spe obtained by the five models in the classification background is opposite to the Rec rate obtained in the classification foreground. Among the five models, the highest Acc is ResNet50 with a value of 92.87%, and the lowest is ViT with a value of 89.26%.

Comparison on Test Set: In Tab. 6 we summarize the results of these five network predictions. we can find that Acc of ResNet50 is the highest (90.00%), Acc of X-Inception is the lowest at 85.85%. Furthermore, the lowest prediction Acc of the transparent foreground is the X-Inception value of 51.8%, and the highest is the ResNet50 value of 62.2%.

In order to more intuitively express the classification results of CNN and ViT models for T-EM image patches, we summarize the confusion matrices predicted by five models into Fig. 7. We find that the ability of CNNs to classify foreground patches of T-EM images is higher than that of ViT. Among them, the best CNN models is Inception-

Table 5
A comparison of the classification results on train and test sets of 8×8 pixel patches. Train (Train times), Test (Test times) and Avg (Single picture prediction time)(In [s]).

| model | Train | Test | Avg | Size(MB) |
|--------------|-------|------|--------|----------|
| ResNet50 | 48762 | 1448 | 0.0067 | 114 |
| Inception-V3 | 61443 | 1186 | 0.0055 | 107 |
| VGG-16 | 49477 | 757 | 0.0035 | 62.2 |
| X-inception | 61247 | 999 | 0.0046 | 103 |
| ViT | 22133 | 1670 | 0.0078 | 31.2 |

V3, which correctly classify 29686 foreground patches, accounting for 91.50% of the total correct foreground patches. ViT correctly classify 27177 foreground patches, accounting for 83.76% of the total correct foreground patches. In addition, the number of correctly classify backgrounds in ResNet50 is at most 165369, accounting for 90.57% of the total correct background patches, and the Pre of the classify background patches is 97.55%. Among the five models, ResNet50 has the highest prediction accuracy rate of 90.06%. To better show the classification results, we reconstruct T-EM images after dicing in Fig. 6.

In Tab. 5, we provide the model training and prediction time and the size of the model during the experiment. From the perspective of model training time, the ViT model is much lower than CNN models, where the ViT training time is 12418 seconds, and the X-Inception training time is the longest 45897 seconds. From the perspective of the size of the model, the minimum size of the ViT model is 31.2M, and the maximum size of the ResNet50 model is 114M. We calculate the time of the five prediction models. The fastest prediction time of VGG-16 is 757 seconds and the prediction time of a single picture is 0.0063 second. The slowest time of ViT is 1670 seconds and the prediction time of a single picture is 0.0078 second.

3.3.2. Comparative Experiment of 224×224 Pixel Patches

Comparison on Training and Validation Sets: We compare the 224×224 pixel patches in the same way as in the previous work in Section 3.1.3. In Tab. 7, we summarize the classification results on validation set of 224×224 pixel patches for each network model. The highest Pre of classification foreground is ResNet50, which is 64.6%, the lowest is X-Inception value of 60.8%. However, the highest Pre of background classification is X-Inception value of 97.9%, and the lowest is ViT value of 96.0%. The highest Rec of the five model classification foreground is that the X-Inception, which is 90.4%, and the lowest is the ViT value of 80.7%. The spe rate obtained by the five models in the classification background is opposite to the Rec rate obtained in the classification foreground. Overall, the Rec and Spe rate of the five model classification backgrounds are almost 90%. When ResNet50 classifies the foreground and background of T-EM images, F1-Score achieves the best result. Meanwhile, the Acc of ResNet50 model training is the highest at



Figure 6: Reconstruction of 8×8 pixel T-EM images classification results.

Table 6

A comparison of the classification results on test set of 8×8 pixel patches. PAcc (prediction accuracy), FG (foreground) and BG (background)(In [%].)

| Model | Class | Pre | Rec | Spe | F1 | PAcc |
|--------------|-------|------|------|------|------|-------|
| ResNet50 | FG | 62.2 | 87.2 | 90.6 | 72.6 | 90.0 |
| | BG | 97.5 | 90.6 | 87.2 | 93.9 | |
| Inception-V3 | FG | 52.6 | 91.5 | 85.4 | 66.8 | 86.29 |
| | BG | 98.3 | 85.4 | 91.5 | 91.4 | |
| VGG-16 | FG | 60.7 | 89.4 | 89.7 | 72.6 | 89.6 |
| | BG | 97.9 | 89.7 | 89.4 | 93.6 | |
| X-Inception | FG | 51.8 | 90.7 | 85.0 | 65.9 | 85.85 |
| | BG | 98.1 | 85.0 | 90.7 | 91.1 | |
| ViT | FG | 60.4 | 83.8 | 90.2 | 70.2 | 89.25 |
| | BG | 96.9 | 90.2 | 83.8 | 93.4 | |

94.99%.

Comparison on Test set: In Tab. 8, we summarize the results of these five network predictions. we can find that the prediction Acc of X-Inception is the highest (89.11%), and the prediction Acc of Inception-V3 is the lowest at 88.10%. However, the highest Pre in predicting transparent foreground is the ViT which is 60.6%.

In order to more intuitively express the classification results of CNN and ViT models on T-EM image patches, we summarize the confusion matrices predicted by five models in Fig. 9. We find that the ability of CNNs to classify foreground patches of T-EM images is higher than that of ViT. Among them, X-Inception is the best in the CNN models, which correctly classifies 29559 small patches. ViT correctly classifies 26285 foreground patches. However, the highest accuracy of classifying T-EM image backgrounds is the ViT, which is 90.52%. It correctly classifies 165288 background images. Meanwhile, in order to better show the classification results, we reconstruct T-EM images after dic-

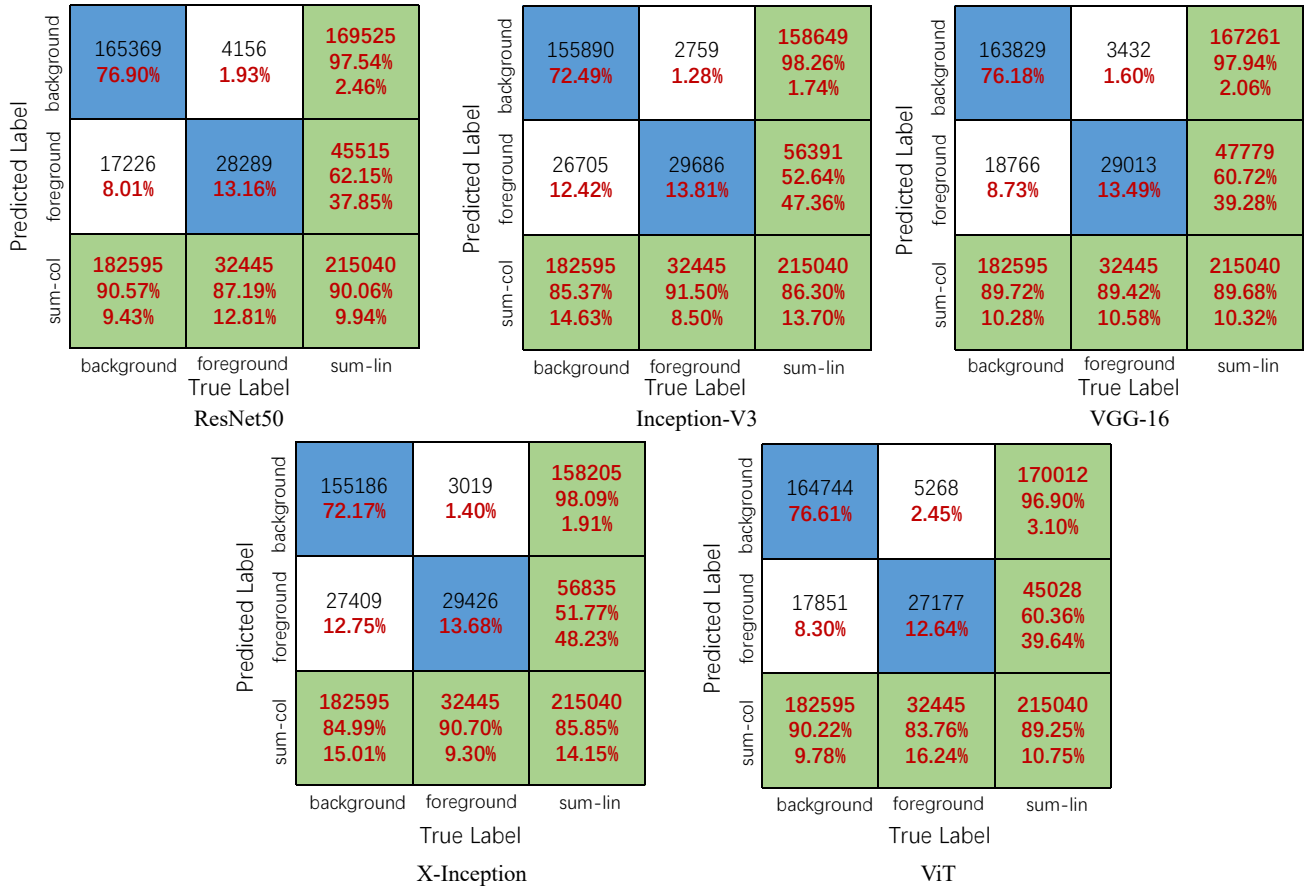


Figure 7: Predict the confusion matrix on test set of 8×8 pixel patches

Table 7

A comparison of the classification results on validation set of 224×224 pixel patches. MAcc (Max Acc), FG (foreground) and BG (background)(In [%].)

| Model | Class | Pre | Rec | Spe | F1 | Max Acc |
|--------------|-------|------|------|------|------|---------|
| ResNet50 | FG | 64.6 | 87.6 | 90.7 | 74.4 | 94.99 |
| | BG | 97.4 | 90.7 | 87.6 | 93.9 | |
| Inception-V3 | FG | 63.0 | 88.9 | 89.9 | 73.7 | 92.51 |
| | BG | 97.7 | 89.9 | 88.9 | 93.6 | |
| VGG-16 | FG | 63.2 | 85.8 | 90.3 | 72.8 | 92.08 |
| | BG | 97.1 | 90.3 | 85.8 | 93.6 | |
| X-Inception | FG | 60.8 | 90.4 | 88.7 | 72.7 | 94.72 |
| | BG | 97.9 | 88.7 | 90.4 | 93.1 | |
| ViT | FG | 63.3 | 80.7 | 90.9 | 70.9 | 89.28 |
| | BG | 96.0 | 90.9 | 80.7 | 93.4 | |

Table 8

A comparison of the classification results on test set of 224×224 pixel patches. PAcc (prediction accuracy), FG (foreground) and BG (background)(In [%].)

| Model | Class | Pre | Rec | Spe | F1 | PAcc |
|--------------|-------|------|------|------|------|-------|
| ResNet50 | FG | 59.0 | 88.7 | 89.0 | 70.9 | 88.92 |
| | BG | 97.8 | 89.0 | 88.7 | 93.2 | |
| Inception-V3 | FG | 56.8 | 90.6 | 87.7 | 69.8 | 88.10 |
| | BG | 98.1 | 87.7 | 90.6 | 92.6 | |
| VGG-16 | FG | 57.1 | 87.0 | 88.3 | 68.9 | 88.11 |
| | BG | 97.4 | 88.3 | 87.0 | 92.6 | |
| X-Inception | FG | 59.6 | 88.0 | 89.3 | 71.1 | 89.11 |
| | BG | 97.6 | 89.3 | 88.0 | 93.3 | |
| ViT | FG | 60.6 | 80.5 | 90.6 | 69.1 | 89.09 |
| | BG | 96.3 | 90.6 | 80.5 | 93.4 | |

In Tab. 9, we find that the training time of the ViT model is still the fastest at 12418 seconds, and the slowest is 73465 seconds for X-Inception. Besides the fastest prediction time of Inception-V3 is 1049 seconds and the prediction time of a single picture is 0.0060 second. The slowest time of ViT is 2156 seconds and the prediction time of a single picture is 0.0100 second.

3.4. In-depth Analysis

We compare classification results in Tab. 4 and Tab. 7, and find that when the T-EM image patches of the training input increase from 8×8 to 224×224 pixels, the Pre of the classification foreground of the five models improves. The biggest improvement is X-Inception from 53.3% to 60.8%. This shows that when the image input size becomes larger,



Figure 8: Reconstruction of 224×224 pixel T-EM images classification results.

Table 9

A comparison of the classification results on train and test sets of 224×224 pixel patches. Train (Train times), Test (Test times) and Avg (Single picture prediction time)(In [s].)

| model | Train | Test | Avg | SIZE(MB) |
|--------------|-------|------|--------|----------|
| ResNet50 | 51077 | 1634 | 0.0076 | 114 |
| Inception-V3 | 66095 | 1296 | 0.0060 | 107 |
| VGG-16 | 50908 | 1364 | 0.0063 | 62.2 |
| X-inception | 73465 | 1049 | 0.0049 | 103 |
| ViT | 23102 | 2156 | 0.0100 | 31.2 |

CNNs can extract more features, thereby improving the model's classification performance for T-EM images. As the input image size increases, it has little effect on the performance of the five models to classify the T-EM image backgrounds. Among them, the biggest improvement is X-Inception, which has an Acc increase of 1.2%. With the increase in the size of the input image of the CNNs, the training time of the five

models has also increase by 2% to 6%, but the Acc of the model has also improve, and the training Acc of the ResNet50 model is the highest value of 94.99%. VGG-16 and ViT remain basically unchange.

We compare Tab. 6 and Tab. 8. When the T-EM image is cropped into pathes of 8×8 pixels, the prediction Acc of the ResNet50 model is the highest value of 90%, and the lowest is the X-Inception value of 85.85%. However, when the T-EM image is enlarged and cropped into patches of 224×224 pixels, the X-Inception prediction Acc rate is the highest 89.11%, and the second is that the ViT Acc rate is 89.09%. By increasing the size of the input T-EM image patches, the prediction Acc of the ViT model exceeds that of ResNet50, Inception-V3 and VGG-16. Moreover, when the input image is a small patches of 224×224 pixels, the Pre of the ViT model to classify the foreground of the T-EM image is higher than that of the CNNs network. This shows that the advantage of ViT for global information description is higher than that of some CNNs networks.

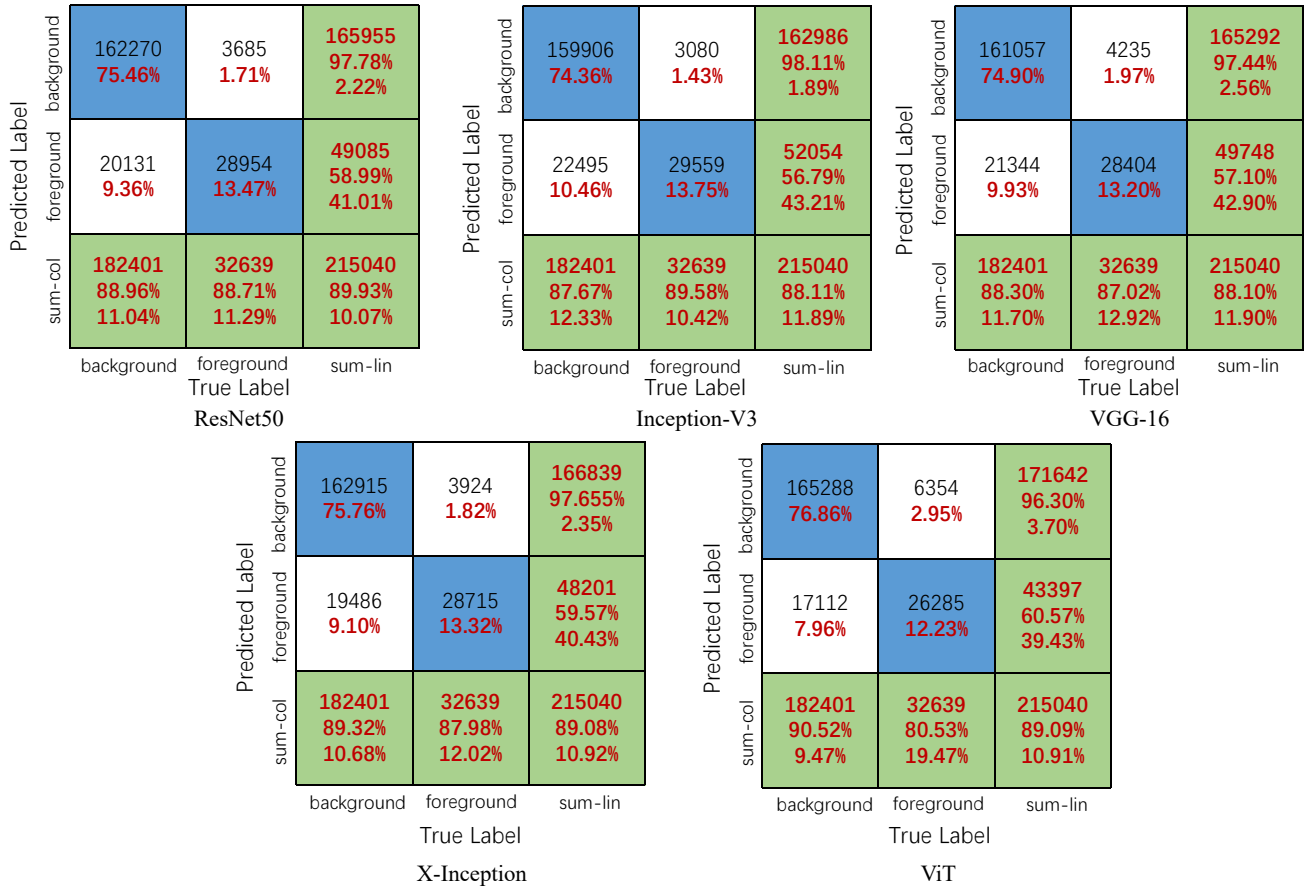


Figure 9: Predict the confusion matrix on test set of 224×224 pixel patches

In the predicted 215040 patches, we compare the performance of five types of network classification foreground and background. In Fig. 7, we find that Inception-v3 has the largest number of correct foregrounds under 8×8 pixel patches. ResNet50 has the largest number of correctly classify backgrounds. In Fig. 9 we find that Inception-v3 has the largest number of correctly classify foregrounds under 224×224 pixel patches, and the largest number of correctly classify background patches is ViT. In addition, the number of foreground patches misclassify by the ViT network model is much smaller than that of the CNNs network. At the same time, the number of correctly classify foreground in the CNNs network is greater than that of the ViT network.

4. Conclusion and Future Work

In this paper, we aim at the problem that T-EM images are difficult to classify by cropping the image into patches and classifying the foreground and background. We use CNNs (ResNet50, Inception-V3, VGG-16, X-Inception) and ViT deep learning methods to compare the performance of classifying patches of T-EM images. In addition, we also compare the effects of patches of 8×8 and 224×224 pixels on the classification performance of deep learning methods. We

conclude that CNNs have better classification performance than ViT in patches of 8×8 pixels. However, the classification performance of ViT at 256×256 pixels is better than that of most CNNs. Therefore, we conclude that CNNs and ViT network models have more advantages in image classification. CNNs are good at extracting local features of images, and ViT is good at extracting images global features.

In the future, we plan to increase the amount of data to improve the stability of the comparison. Meanwhile, the images reconstructed by deep learning classification can be extended to the positioning, segmentation, recognition, and detection of T-EM images. We will further strengthen the application of results.

5. Acknowledgements

This work is supported by National Natural Science Foundation of China (No. 61806047). We thank Miss Zixian Li and Mr. Guoxian Li for their important discussion.

References

- [1] Zihan Li, Chen Li, Yudong Yao, Jinghua Zhang, Md Mamunur Rahman, Hao Xu, Frank Kulwa, Bolin Lu, Xuemin Zhu, and Tao Jiang.

- Emsd-5: Environmental microorganism image dataset fifth version for multiple image analysis tasks. *Plos one*, 16(5):e0250631, 2021.
- [2] May Phylo Khaing and Mukunoki Masayuki. Transparent object detection using convolutional neural network. In *International Conference on Big Data Analysis and Deep Learning Applications*, pages 86–93. Springer, 2018.
 - [3] Jay Martin Tenenbaum. Accommodation in computer vision. Technical report, Stanford Univ Ca Dept of Computer Science, 1970.
 - [4] Michael Isard and Andrew Blake. Contour tracking by stochastic propagation of conditional density. In *European conference on computer vision*, pages 343–356. Springer, 1996.
 - [5] Michael D Kelly. Edge detection in pictures by computer using planning. Technical report, STANFORD UNIV CALIF DEPT OF COMPUTER SCIENCE, 1970.
 - [6] Vicki Bruce and Andy Young. Understanding face recognition. *British journal of psychology*, 77(3):305–327, 1986.
 - [7] Pierre Baldi and Yves Chauvin. Neural networks for fingerprint recognition. *neural computation*, 5(3):402–418, 1993.
 - [8] Sorin Grigorescu, Bogdan Trasnea, Tiberiu Cocias, and Gigel Macesanu. A survey of deep learning techniques for autonomous driving. *Journal of Field Robotics*, 37(3):362–386, 2020.
 - [9] Dinggang Shen, Guorong Wu, and Heung-Il Suk. Deep learning in medical image analysis. *Annual review of biomedical engineering*, 19:221–248, 2017.
 - [10] Bernd Jähne and Horst Haußecker. Computer vision and applications. 2000.
 - [11] Joao Carreira, Henrique Madeira, and Joao Gabriel Silva. Xception: A technique for the experimental evaluation of dependability in modern computers. *IEEE Transactions on Software Engineering*, 24(2):125–136, 1998.
 - [12] Qing Guan, Yunjun Wang, Bo Ping, Duanshu Li, Jiajun Du, Yu Qin, Hongtao Lu, Xiaochun Wan, and Jun Xiang. Deep convolutional neural network vgg-16 model for differential diagnosing of papillary thyroid carcinomas in cytological images: a pilot study. *Journal of Cancer*, 10(20):4876, 2019.
 - [13] A Sai Bharadwaj Reddy and D Sujitha Juliet. Transfer learning with resnet-50 for malaria cell-image classification. In *2019 International Conference on Communication and Signal Processing (ICCSP)*, pages 0945–0949. IEEE, 2019.
 - [14] Xiaoling Xia, Cui Xu, and Bing Nan. Inception-v3 for flower classification. In *2017 2nd International Conference on Image, Vision and Computing (ICIVC)*, pages 783–787. IEEE, 2017.
 - [15] Hong-Yen Chen and Chung-Yen Su. An enhanced hybrid mobilenet. In *2018 9th International Conference on Awareness Science and Technology (iCAST)*, pages 308–312. IEEE, 2018.
 - [16] Fredy Martínez, Fernando Martínez, and Edwar Jacinto. Performance evaluation of the nasnet convolutional network in the automatic identification of covid-19. *Int J Adv Sci Eng Inform Technol*, 10(2):662, 2020.
 - [17] Ashish Vaswani, Noam Shazeer, Niki Parmar, Jakob Uszkoreit, Llion Jones, Aidan N Gomez, Lukasz Kaiser, and Illia Polosukhin. Attention is all you need. *arXiv preprint arXiv:1706.03762*, 2017.
 - [18] Mekapogu Madakka, Nadimikeri Jayaraju, Nambi Rajesh, and Muni Ramanna Gari Subhosh Chandra. Development in the treatment of municipal and industrial wastewater by microorganism. In *Recent developments in applied microbiology and biochemistry*, pages 263–273. Elsevier, 2019.
 - [19] Stefania Bambini and Rino Rappuoli. The use of genomics in microbial vaccine development. *Drug discovery today*, 14(5-6):252–260, 2009.
 - [20] Andrew C Chapple, Roger A Downer, and Roy P Bateman. Theory and practice of microbial insecticide application. In *Field manual of techniques in invertebrate pathology*, pages 5–37. Springer, 2000.
 - [21] Hao Xu, Chen Li, Md Mamunur Rahaman, Yudong Yao, Zihan Li, Jinghua Zhang, Frank Kulwa, Xin Zhao, Shouliang Qi, and Yueyang Teng. An enhanced framework of generative adversarial networks (ef-gans) for environmental microorganism image augmentation with limited rotation-invariant training data. *IEEE Access*, 8:187455–187469, 2020.
 - [22] Laurent Dufossé. Microbial production of food grade pigments. *Food technology and Biotechnology*, 44(3):313–323, 2006.
 - [23] Andy Zeng, Kuan-Ting Yu, Shuran Song, Daniel Suo, Ed Walker, Alberto Rodriguez, and Jianxiong Xiao. Multi-view self-supervised deep learning for 6d pose estimation in the amazon picking challenge. In *2017 IEEE international conference on robotics and automation (ICRA)*, pages 1386–1383. IEEE, 2017.
 - [24] Shreeyak Sajjan, Matthew Moore, Mike Pan, Ganesh Nagaraja, Johnny Lee, Andy Zeng, and Shuran Song. Clear grasp: 3d shape estimation of transparent objects for manipulation. In *2020 IEEE International Conference on Robotics and Automation (ICRA)*, pages 3634–3642. IEEE, 2020.
 - [25] Zheng Chunjiao. The application and development of photoelectric sensor. In *Intelligence Computation and Evolutionary Computation*, pages 671–677. Springer, 2013.
 - [26] Seiji Hata, Yoko Saitoh, Syoji Kumamura, and Ken’ichi Kaida. Shape extraction of transparent object using genetic algorithm. In *Proceedings of 13th International Conference on Pattern Recognition*, volume 4, pages 684–688. IEEE, 1996.
 - [27] Yichao Xu, Hajime Nagahara, Atsushi Shimada, and Rin-ichiro Taniguchi. Transcut: Transparent object segmentation from a light-field image. In *Proceedings of the IEEE International Conference on Computer Vision*, pages 3442–3450, 2015.
 - [28] Yuanhao Guo, Zhan Xiong, and Fons J Verbeek. An efficient and robust hybrid method for segmentation of zebrafish objects from bright-field microscope images. *Machine vision and applications*, 29(8):1211–1225, 2018.
 - [29] Abozar Nasirahmadi and Seyed-Hassan Miraei Ashtiani. Bag-of-feature model for sweet and bitter almond classification. *Biosystems engineering*, 156:51–60, 2017.
 - [30] Yichao Xu, Kazuki Maeno, Hajime Nagahara, Atsushi Shimada, and Rin-ichiro Taniguchi. Light field distortion feature for transparent object classification. *Computer Vision and Image Understanding*, 139:122–135, 2015.
 - [31] Karen Simonyan and Andrew Zisserman. Very deep convolutional networks for large-scale image recognition. *arXiv preprint arXiv:1409.1556*, 2014.
 - [32] Kaiming He, Xiangyu Zhang, Shaoqing Ren, and Jian Sun. Deep residual learning for image recognition. In *Proceedings of the IEEE conference on computer vision and pattern recognition*, pages 770–778, 2016.
 - [33] Christian Szegedy, Wei Liu, Yangqing Jia, Pierre Sermanet, Scott Reed, Dragomir Anguelov, Dumitru Erhan, Vincent Vanhoucke, and Andrew Rabinovich. Going deeper with convolutions. In *Proceedings of the IEEE conference on computer vision and pattern recognition*, pages 1–9, 2015.
 - [34] Sergey Ioffe and Christian Szegedy. Batch normalization: Accelerating deep network training by reducing internal covariate shift. In *International conference on machine learning*, pages 448–456. PMLR, 2015.
 - [35] Christian Szegedy, Vincent Vanhoucke, Sergey Ioffe, Jon Shlens, and Zbigniew Wojna. Rethinking the inception architecture for computer vision. In *Proceedings of the IEEE conference on computer vision and pattern recognition*, pages 2818–2826, 2016.
 - [36] François Chollet. Xception: Deep learning with depthwise separable convolutions. In *Proceedings of the IEEE conference on computer vision and pattern recognition*, pages 1251–1258, 2017.
 - [37] Alexey Dosovitskiy, Lucas Beyer, Alexander Kolesnikov, Dirk Weissenborn, Xiaohua Zhai, Thomas Unterthiner, Mostafa Dehghani, Matthias Minderer, Georg Heigold, Sylvain Gelly, et al. An image is worth 16x16 words: Transformers for image recognition at scale. *arXiv preprint arXiv:2010.11929*, 2020.